NOTE

Magnetic Resonance in Medicine 00:000–000 (2013)

Accelerated Isotropic Sub-Millimeter Whole-Heart Coronary MRI: Compressed Sensing Versus Parallel Imaging

Mehmet Akçakaya,[1] Tamer A. Basha,[1] Raymond H. Chan,[1] Warren J. Manning,[1,2] and Reza Nezafat[1]*

Purpose: To enable accelerated isotropic sub-millimeter whole-heart coronary MRI within a 6-min acquisition and to compare this with a current state-of-the-art accelerated imaging technique at acceleration rates beyond what is used clinically.

Methods: Coronary MRI still faces major challenges, including lengthy acquisition time, low signal-to-noise-ratio (SNR), and suboptimal spatial resolution. Higher spatial resolution in the sub-millimeter range is desirable, but this results in increased acquisition time and lower SNR, hindering its clinical implementation. In this study, we sought to use an advanced B_1-weighted compressed sensing technique for highly accelerated sub-millimeter whole-heart coronary MRI, and to compare the results to parallel imaging, the current-state-of-the-art, where both techniques were used at acceleration rates beyond what is used clinically. Two whole-heart coronary MRI datasets were acquired in seven healthy adult subjects (30.3 ± 12.1 years; 3 men), using prospective 6-fold acceleration, with random undersampling for the proposed compressed sensing technique and with uniform undersampling for sensitivity encoding reconstruction. Reconstructed images were qualitatively compared in terms of image scores and perceived SNR on a four-point scale (1 = poor, 4 = excellent) by an experienced blinded reader.

Results: The proposed technique resulted in images with clear visualization of all coronary branches. Overall image quality and perceived SNR of the compressed sensing images were significantly higher than those of parallel imaging ($P = 0.03$ for both), which suffered from noise amplification artifacts due to the reduced SNR.

Conclusion: The proposed compressed sensing-based reconstruction and acquisition technique for sub-millimeter whole-heart coronary MRI provides 6-fold acceleration, where it outperforms parallel imaging with uniform undersampling. **Magn Reson Med 000:000–000, 2013. © 2013 Wiley Periodicals, Inc.**

Key words: compressed sensing; accelerated imaging; parallel imaging; whole-heart coronary MRI; sub-millimeter; high resolution imaging

INTRODUCTION

Coronary artery disease remains the leading cause of death in the United States, accounting for one of every six deaths, despite significant efforts in prevention and treatment (1). The current clinical gold standard for the diagnosis of coronary artery disease is catheter-based invasive X-ray angiography. A recent study of nearly 400,000 patients referred for X-ray coronary angiography showed that only less than 40% had obstructive coronary artery disease, a relatively low yield for an invasive test (2). Therefore, alternative noninvasive imaging modalities, such as multi-detector computed tomography and coronary MRI has the potential to be a gate-keeper to invasive coronary X-ray angiography. Coronary multi-detector computed tomography has the advantage of rapid imaging and superior isotropic spatial resolution on the order of $0.6 \times 0.6 \times 0.6$ mm^3. Coronary MRI, on the other hand, is advantageous to multi-detector computed tomography in several respects, as it does not require ionizing radiation or iodinated contrast, thereby facilitating follow-up scanning, and it has smaller artifacts related to epicardial calcium.

Though there have been advances over the last decade, coronary MRI remains challenging due to long scan times, limited spatial resolution, low signal-to-noise-ratio (SNR), and low blood-myocardium contrast-to-noise-ratio. Several approaches have been used to address these limitations, including the application of T_2 magnetization preparation technique (3,4), more efficient k-space sampling (5,6), administration of vasodilators (7), imaging at higher magnetic field strengths (8–10), and the use of exogenous contrast agents (11–21). Recently, it was shown that a sub-millimeter (sub-mm) acquisition with a spatial resolution of $0.35 \times 0.35 \times 1.5$ mm^3 may allow for improved detection of stenosis for targeted coronary MRI (22). However, such high-resolution targeted acquisitions require a 9-min scan time per vessel assuming 100% navigator gating efficiency. A whole-heart coronary MRI scan with 1 mm isotropic spatial resolution results in a 16-min acquisition time assuming a heart rate of 70 bpm and 100% navigator gating efficiency.

[1]Department of Medicine (Cardiovascular Division), Beth Israel Deaconess Medical Center and Harvard Medical School, Boston, Massachusetts, USA.
[2]Department of Radiology, Beth Israel Deaconess Medical Center and Harvard Medical School, Boston, Massachusetts, USA.

Grant sponsor: NIH; Grant numbers: R01EB008743-01A2; K99HL111410-01.

*Correspondence to: Reza Nezafat, Ph.D., Beth Israel Deaconess Medical Center, 330 Brookline Ave, Boston, MA 02215. E-mail: rnezafat@bidmc.harvard.edu

Received 30 November 2012; revised 11 January 2013; accepted 17 January 2013

DOI 10.1002/mrm.24683
Published online 00 Month 2013 in Wiley Online Library (wileyonlinelibrary.com).

Thus, to achieve whole-heart coverage and sub-mm isotropic spatial resolution, accelerated imaging is required.

Non-Cartesian trajectories (23), or parallel imaging techniques such as generalized autocalibrating partially-parallel acquisition (GRAPPA) (18,20) or sensitivity encoding (SENSE) (19,24) have been used in previous studies to reduce the scan time of coronary MRI, with resultant acceleration rates of up to 2-fold while using 5 to 16 element cardiac-coil arrays, and up-to 4-fold acceleration rate using 32-channel coils (25,26). Currently, parallel imaging is considered the state-of-the-art accelerated imaging technique for whole-heart coronary MRI and is commonly used for clinical imaging.

Compressed sensing (CS) is an alternative image reconstruction method for accelerated acquisitions with incoherently undersampled k-space data that exploits the sparsity of the image in a transform domain (27,28). CS requires an incoherent undersampling pattern, which can be achieved by random undersampling of k-space data in the k_y–k_z plane for three-dimensional Cartesian acquisitions. In pediatric MRI, a combination of CS and parallel imaging outperforms parallel imaging alone, when a randomly undersampled k-space is used for both reconstruction techniques (29). In high-resolution CMR, an improved CS-based reconstruction strategy for randomly undersampled data, called low-dimensional-structure self-learning and thresholding (LOST) provides reconstructions with reduced blurring compared with conventional CS techniques (30) and was successfully used in contrast-enhanced whole-heart coronary MRI (21), as well as accelerated isotropic resolution late gadolinium enhancement imaging (31). Although these studies have demonstrated that a prospectively randomly undersampled k-space with CS reconstruction can be used clinically, a head-to-head comparison of such CS techniques using prospective random k-space undersampling versus parallel imaging with prospective uniform undersampling has not been performed.

In this study, we sought to enable highly accelerated acquisition of sub-mm resolution (0.9 mm isotropic) whole-heart coronary MRI, using a prospective random undersampling of k-space and an image reconstruction technique combining parallel imaging and LOST, thereby reducing the scan time to ~6 min. We further sought to compare this CS technique to parallel imaging with uniform undersampling, the current state-of-the-art in accelerated coronary MRI, where both techniques were used at acceleration rates beyond what is used clinically.

METHODS

All imaging sequences were implemented on a 1.5-T Philips Achieva (Philips Healthcare, Best, The Netherlands) system with a 32-channel cardiac phased-array receiver coil. For this HIPAA-compliant study, the imaging protocol was approved by our institutional review board. Written informed consent was obtained from all participants.

Accelerated Sub-mm Coronary MRI

Seven healthy adult subjects (30.3 ± 12.1 years, 3 men) underwent coronary MRI. Scout images were acquired with a steady state free precession sequence with 3.1×3.1 mm^2 in-plane resolution and 10 mm slice thickness. This was followed by a breath-held high-temporal-resolution cine steady state free precession image in the two-chamber view (pulse repetition time/echo time = 3.7/1.8 ms; temporal resolution = 48 ms; spatial resolution = 1.7×1.7 mm^2) to visually identify the quiescent period of the right coronary artery (RCA), which was subsequently used as the electrocardiogram trigger delay for whole-heart coronary MRI. A subject-specific acquisition window was used, ranging between 80 and 125 ms.

Whole-heart coronary MRI was acquired using a free-breathing electrocardiogram-triggered navigator-gated steady state free precession sequence with isotropic sub-mm spatial resolution ($0.9 \times 0.9 \times 0.9$ mm^3). Images were acquired in the coronal plane with a field-of-view = $290 \times 290 \times 100$ mm^3. A truncated radiofrequency excitation pulse (flip angle = 90°) was used for a reduced repetition time and echo time of 4.0 ms and 2.0 ms, respectively. A T_2 magnetization preparation pulse (echo time = 50 ms) and a spectrally selective fat-saturation sequence were used to improve contrast between coronary arteries and surrounding myocardium and fat. A navigator placed on the dome of the right hemidiaphragm was used for respiratory motion compensation, using prospective real-time correction with a 5 mm end-expiration gating window and 0.6 superior-inferior tracking ratio (32,33). Saturation bands were used to reduce fold-over artifacts in the phase encode direction.

Two separate accelerated acquisitions were performed for this study. For the SENSE-based approach, the data acquisition was prospectively accelerated using uniform undersampling (3-fold in k_y and 2-fold k_z), using the commercially available pulse sequence. For the LOST-based approach, the data acquisition was prospectively accelerated by a rate of 6 in k_y–k_z using a pseudo-randomly generated undersampling pattern. Central k-space corresponding to 3% of the k-space was fully sampled, and the outer k-space was randomly undersampled. A modified radial k_y–k_z phase reordering scheme was used to mitigate flow artifacts and Eddy currents by reducing gradient switching (21). A brief description of this technique is available in Appendix A. The order of the two accelerated acquisitions was randomized.

Image Reconstruction

The acquired raw data for the randomly undersampled CS acquisitions were exported from the scanner and images were reconstructed offline using an iterative B_1-weighted LOST algorithm. In a previous study, LOST algorithm was shown to improve on existing CS methods in terms of image sharpness for coronary MRI (30). Briefly, in this approach, an image estimate is used to adaptively identify two-dimensional image blocks of similar signal content, which are grouped into similarity clusters. For each voxel of the image, the $N_b \times N_b$ reference block whose top left corner is at that voxel is compared using the normalized l_2 distance to another block. These blocks are declared to be similar if this distance is less than a threshold, λ_{match}, and the compared block is added to the similarity cluster of that voxel. Then, a three-dimensional fast Fourier transform is applied to

each similarity cluster to adaptively sparsify the data (30). Thresholding of the data is performed via the shrinkage of the three-dimensional fast Fourier transform coefficients of the similarity clusters.

In the iterative B_1-weighted reconstruction approach, the coil sensitivity information is used for data consistency during the reconstruction (34,35). Coil sensitivity maps were generated from the fully sampled central k-space using Hanning filtering in the k_y–k_z direction. At every iteration of the B_1-weighted LOST algorithm: (1) The current combined-coil image estimate was thresholded using LOST as described, (2) The combined image was mapped to individual coils via voxel-wise multiplication with the sensitivity map of that coil, (3) Data consistency with the measured data was enforced by Fourier transforming the coil images, replacing the acquired k-space locations with the acquired lines, and inverse Fourier transforming to get data-consistent images, (4) The data-consistent coil images were combined using the coil sensitivity maps, where the voxel-wise product of the coil images and conjugate of the coil sensitivity maps were summed across the coil dimension, to generate the next image estimate. The algorithm is summarized in Figure 1.

LOST reconstruction was implemented in Matlab (v7.6, MathWorks, Natick, MA), with the adaptive learning and nonlinear shrinkage portions implemented in C++. The details of the implementation, as well as the reconstruction parameters are described in Appendix B. The same reconstruction parameters were used in all cases, allowing for fully automated reconstructions. Comparison images for SENSE were generated using the commercially available scanner software. The reconstruction resolution for the final LOST images and the SENSE images was $0.45 \times 0.45 \times 0.45$ mm^3.

Image and Statistical Analysis

Subjective image scores were used to evaluate the LOST and SENSE reconstructions for all datasets. A qualitative assessment of coronary artery image quality was performed by an experienced independent blinded reader with coronary MRI experience, using a four-point scale system (36): 1, poor or uninterpretable (coronary artery visible, with markedly blurred borders and edges); 2, fair (coronary artery visible, with moderately blurred borders and edges); 3, good (coronary artery visible, with mildly blurred borders and edges); 4, excellent (coronary artery visible, with sharply defined borders and edges). Separate scores were given for the proximal, mid, and distal segments of the RCA, the left anterior descending artery (LAD) and the left circumflex artery (LCX); and for the left main artery. Additionally, an overall image score for the visualization of coronaries was given for each subject. Due to the difficulty of SNR quantification for CS techniques, which inherently threshold and shrink the noise, a perceived SNR score was given (29) on a four-point scale (1, lowest; 4, highest). The signed rank test was used for imaging scores to test for the null hypothesis that the central tendency of the difference was zero

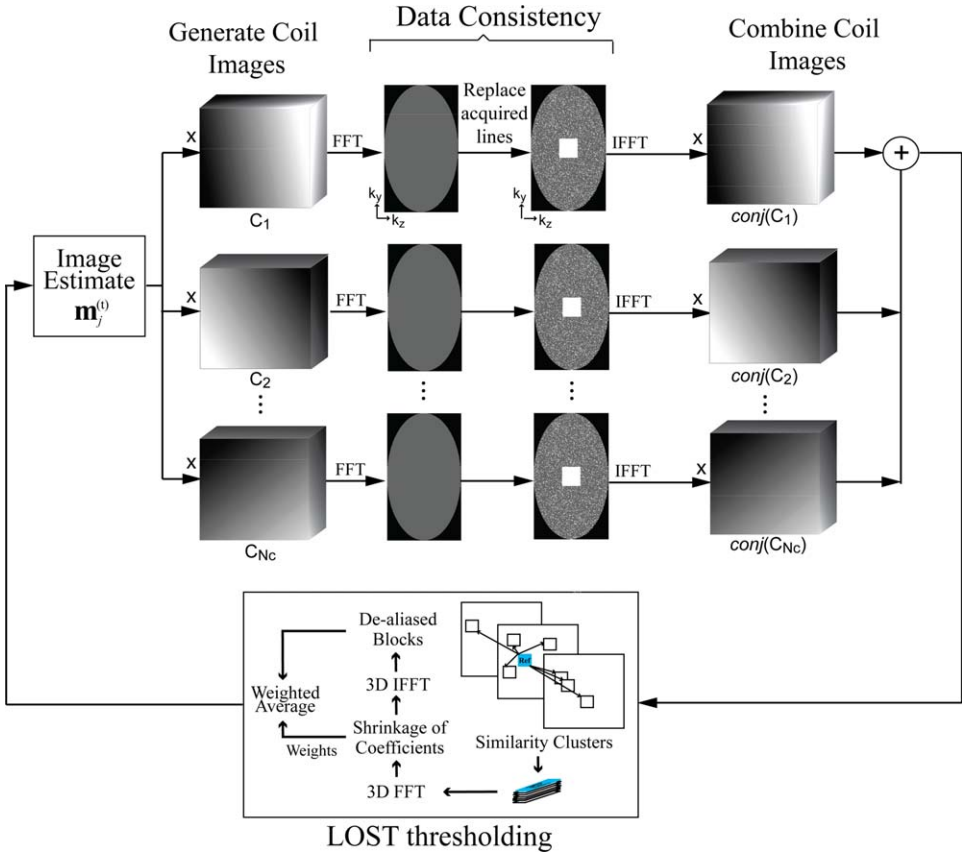

FIG. 1. Schematic for a single iteration of the B_1-weighted LOST algorithm used in this study. At every iteration, the current image estimate is mapped to individual coil images by voxel-wise multiplication with sensitivity maps. Data consistency is enforced by replacing the acquired k-space lines. A combined image is generated by summing the voxel-wise product of data-consistent coil images and conjugate of coil sensitivity maps across the coil dimension. This image is then thresholded using LOST. The implementation details of LOST thresholding are given in Appendix B.

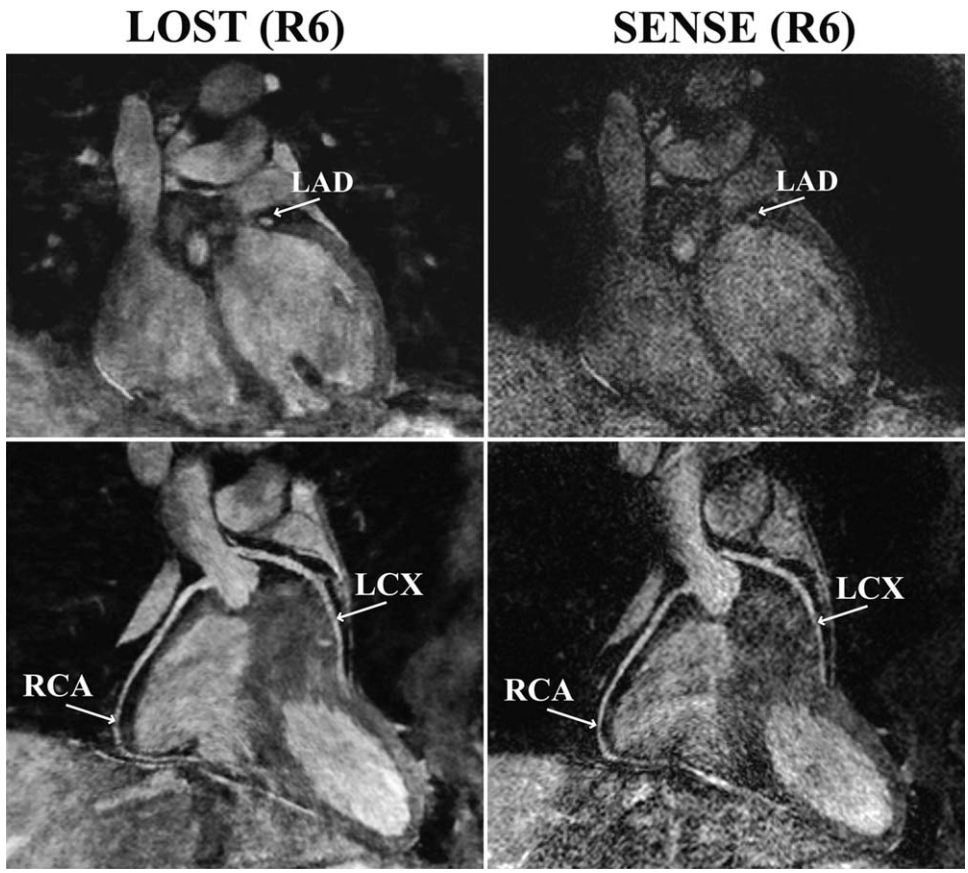

FIG. 2. An example coronal slice (top) and reformatted coronal image (bottom) of a subject using B_1-weighted LOST with 6-fold random undersampling (left) and SENSE with 6-fold uniform undersampling. A cross-section of the LAD is visualized clearly with the proposed technique, whereas noise amplification is apparent in the SENSE-reconstructed image (RCA: right coronary artery, LAD: left anterior descending, LCX: left circumflex).

for the two reconstructions. All statistical analyses were performed using SAS (v9.3, SAS Institute, Cary, NC). A P value of < 0.05 was considered to be significant.

A SoapBubble tool (37) was used to quantitatively evaluate vessel sharpness for RCA, LAD, and LCX, using the proximal and mid segments. Vessel sharpness scores were calculated for both sides of the vessel using a Deriche algorithm (38). Final normalized sharpness was defined as the average score of both sides divided by the center of vessel intensity.

RESULTS

Sub-mm whole-heart coronary MRI scanning was successfully completed in all subjects with both methods and without complications. The nominal scan time for these acquisitions was 3:30 min at 70 heart-beats per min, assuming 100% navigator gating efficiency. The average scan time was $6{:}06 \pm 1{:}24$ min (range 3:56 and 7:40 min) for LOST, and $6{:}09 \pm 1{:}13$ (range 4:32 to 7:39 min) for SENSE ($P =$ NS). The corresponding average navigator gating efficiencies were $59.7 \pm 13.1\%$ (range: 49.5% and 86.5%) and $58.0 \pm 8.5\%$ (range: 50.5% and 75.1%), respectively ($P =$ NS), with an overall average navigator gating efficiency of $58.8 \pm 10.6\%$. The difference between the nominal scan time and the actual average scan time are due to differences in breathing patterns and heart rates of the subjects. The reconstruction time for the B_1-weighted LOST algorithm was $\sim$ 90 min.

Figure 2 depicts an example coronal slice and reformatted coronal image from one of the acquisitions, showing a cross-section of the LAD, and long axis of the RCA and LCX of the subject respectively, reconstructed with LOST and SENSE. The LAD is clearly visualized in the coronal cross-section with the proposed B_1-weighted LOST approach, whereas noise amplification in the SENSE image is apparent, and the visualization of the LAD is hindered. The reformatted images also show the different levels of noise amplification, although the effect is less visible due to the reformatting. Figure 3 shows axial reformats from a different subject. Both noise amplification and folding artifacts in the anterior–posterior direction are visible in the SENSE images depicting the proximal RCA and LAD. These artifacts are not produced with the LOST approach, where both branches are visualized clearly. Example coronal cross-section and reformatted coronal slices in another subject are depicted in Figure 4, which demonstrate high levels of noise amplification in the SENSE reconstruction. In this case, the left main coronary artery is not visible due to noise, and the proximal LCX and distal RCA cannot be tracked for reformatting in the SENSE images. All the coronary arteries, including the distal sections are shown with improved definition using the LOST approach.

Table 1 summarizes the qualitative coronary MRI assessment for the LOST and the SENSE reconstructions from the randomly undersampled and uniformly undersampled acquisitions respectively. The scores for all coronary artery branches were higher for LOST, although

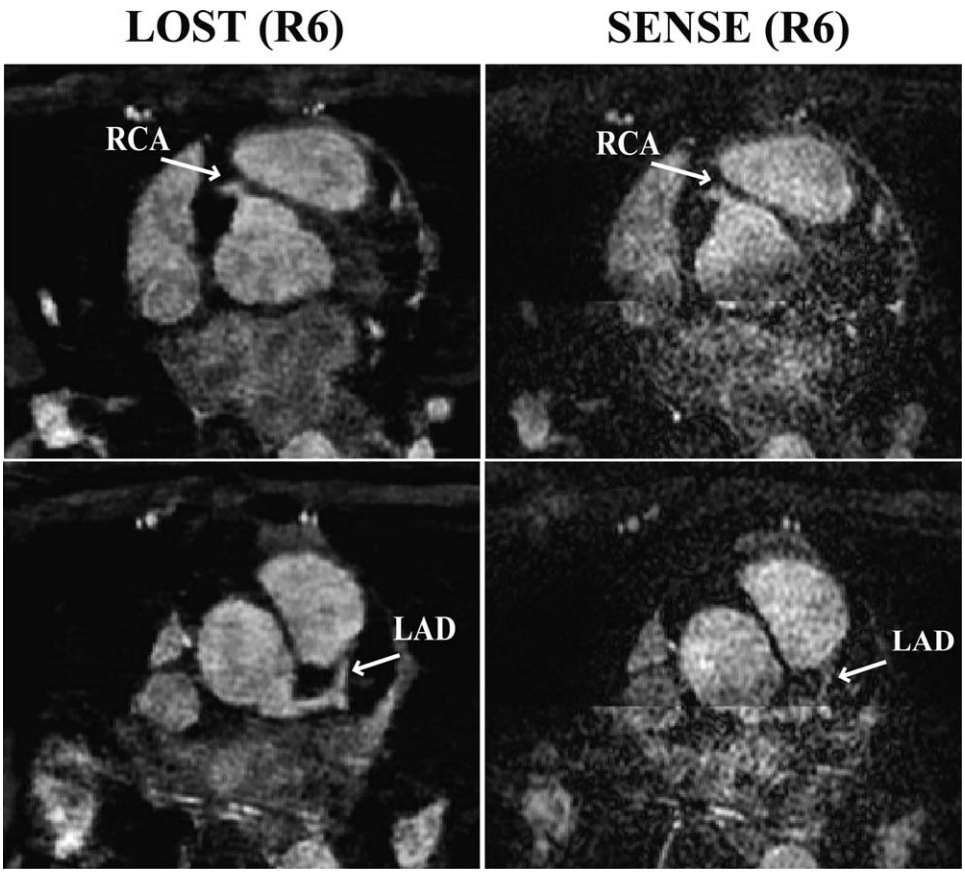

FIG. 3. Example axial reformats using B_1-weighted LOST with 6-fold random undersampling (left) and SENSE with 6-fold uniform undersampling. Noise amplification and SENSE folding artifacts in the *z*-direction (anterior–posterior) are apparent in both of the slices depicting the proximal RCA and the proximal LAD. Similar artifacts are not visible in the proposed LOST technique.

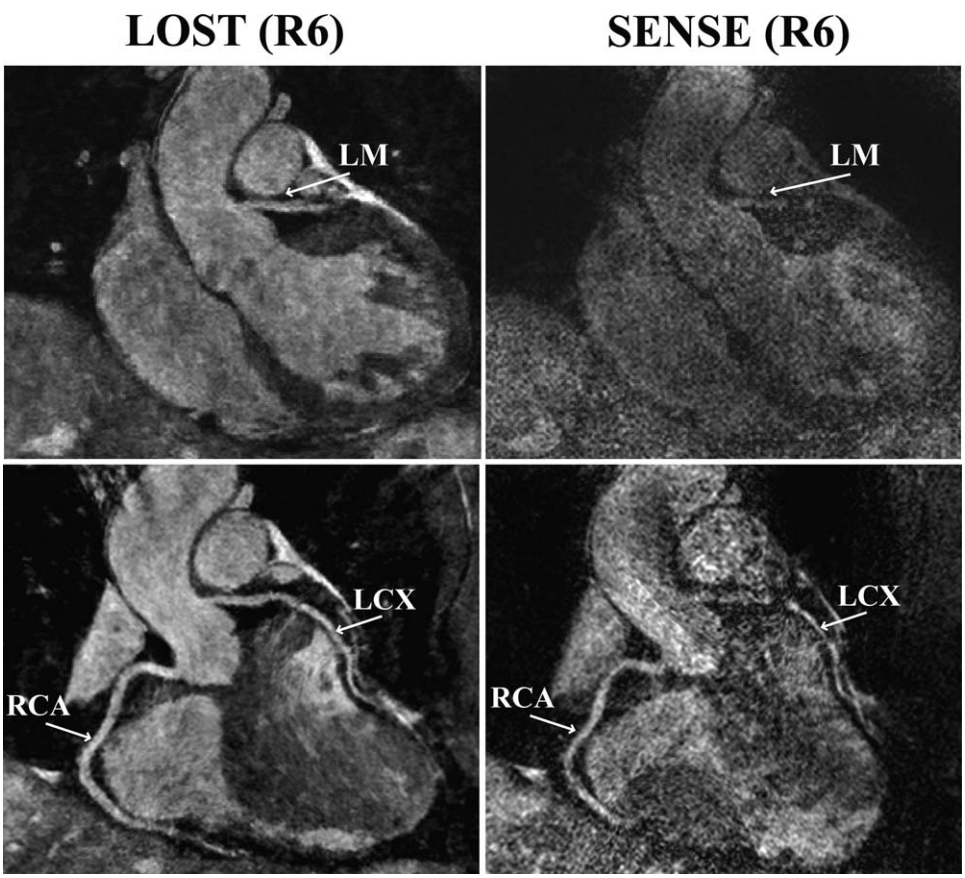

FIG. 4. An example coronal slice (top) containing a cross-section of the left main shows that SENSE images with 6-fold uniform undersampling (right) suffers from noise amplification, whereas the left main is clearly visualized using B_1-weighted LOST with 6-fold random undersampling (left). In the reformatted coronal images (bottom), the proximal LCX cannot be tracked due to the high noise level in the SENSE reconstruction, but RCA and LCX branches are visualized with the LOST technique.

Table 1
Comparison of average subjective imaging scores (1 = poor, 2 = fair, 3 = good, 4 = excellent) between SENSE reconstruction with 6-fold uniform undersampling and B1-weighted LOST reconstruction with 6-fold random undersampling.

	PROXIMAL			MID			DISTAL					
	RCA	LAD	LCX	RCA	LAD	LCX	RCA	LAD	LCX	LM	OVERALL	PERCEIVED SNR
SENSE	3.1 ± 0.9	2.4 ± 1.3	2.4 ± 1.3	2.3 ± 1.1	2.6 ± 1.3	1.9 ± 0.9	2.3 ± 1.1	2.3 ± 1.0	1.7 ± 1.0	2.7 ± 1.1	2.1 ± 0.9	2.4 ± 1.1
LOST	3.6 ± 0.5	3.7 ± 0.5	3.4 ± 0.8	3.0 ± 0.8	3.1 ± 0.7	2.7 ± 0.8	2.6 ± 1.1	3.0 ± 1.2	2.0 ± 1.3	3.7 ± 0.5	3.1 ± 0.7	3.4 ± 0.8
P value	0.50	0.06	0.06	0.18	0.31	0.03	0.63	0.06	0.50	0.06	0.03	0.03

LOST was evaluated higher for all branches. The differences were statistically significant for overall score and perceived SNR score, as well as the mid-LCX. A *P*-value less than 0.05 was considered significant.

the difference was statistically significant for only the mid LCX branch. The overall image score for LOST was significantly higher than that of SENSE (3.1 ± 0.7 vs. 2.1 ± 0.9, $P = 0.03$). The perceived SNR score was also significantly higher for LOST (3.4 ± 0.8 vs. 2.4 ± 1.1, $P = 0.03$). Vessel sharpness measurements were completed on all subjects, except two, where the LAD and LCX were not visible in the SENSE images. These coronary branches of the two subjects were excluded from further analysis. The vessel sharpness values for LOST and SENSE were as follows: 0.60 ± 0.06 vs. 0.57 ± 0.06 ($P = 0.02$) for the RCA ($N = 7$); 0.61 ± 0.05 vs. 0.59 ± 0.05 ($P = 0.18$) for the LAD ($N = 5$); 0.61 ± 0.06 vs. 0.59 ± 0.03 ($P = 0.17$) for the LCX ($N = 5$).

DISCUSSION

In this study, we have demonstrated the efficacy of an accelerated isotropic sub-mm whole-heart coronary MRI method using a prospective random undersampling scheme and the B_1-weighted LOST reconstruction technique. These reconstruction and acquisition techniques allow for high-quality visualization of all coronary branches, with 6-fold accelerated acquisitions. Among a healthy group of subjects, the technique was found to be superior to parallel imaging with uniform undersampling in terms of overall quality and perceived SNR at the same acceleration rate.

CS techniques have been used in numerous MRI applications; however, its usage in clinical settings has been limited, as its advantages over existing methods have not been clearly demonstrated. Much work on CS has been based on reconstruction techniques with retrospective undersampling of fully sampled data, which fails to capture realistic scenarios. Prospective Cartesian random undersampling has been used in previous studies (21,29,39–43). Furthermore, comparison to parallel imaging have also been provided, where the parallel imaging reconstruction has been used with the same random undersampling pattern (29), although this approach results in performance deterioration for parallel imaging techniques (44). Hence, use of uniform undersampling for parallel imaging techniques is important for a fair comparison between these techniques. In an earlier study, comparison examples between SENSE with a uniformly undersampled acquisition and CS with prospectively random undersampled acquisition were provided (30); however, a thorough comparison between the two methods were not performed. To the best of our knowledge, this work provides the first detailed head-to-head comparison between CS with prospective random undersampling and parallel imaging with prospective uniform undersampling in high-resolution cardiac MR, and highlights the advantages of CS methods for highly accelerated low SNR applications.

The qualitative image scores indicate that the proposed method performs particularly well in proximal and mid segments, where the most clinically significant lesions occur (36). Distal segments were scored lower for both accelerated techniques, presumably because of the low SNR and contrast-to-noise-ratio in these segments due to the high spatial resolution. Contrast agents have been shown to improve SNR and contrast-to-noise-ratio in the distal branches of the coronaries (19). In this study, we used a noncontrast enhanced coronary MRI technique to allow for two acquisitions with different undersampling patterns, without being affected by contrast washout and changes in inversion time. Use of contrast agents may improve the visibility of the distal branches, however the usage of a contrast-enhanced coronary MRI sequence at this spatial resolution was not studied.

Although vessel sharpness measurements were provided in this study, these may not be a good indicator of image quality in this setting for a number of reasons. First, the SENSE reconstruction is processed by the commercial reconstruction software, which applies additional filters that are not available on the raw data that is used to reconstruct the CS images. Second, vessel sharpness does not necessarily provide information about noise, the main source of difference of image quality in this study, as exemplified by the discrepancy between the perceived SNR and the vessel sharpness measurements. However, the measurements were included for completeness, but its usage in comparing reconstructions from different acquisitions with different processing may be limited.

Our study has several limitations. Only a small number of healthy adult subjects were studied. Further studies are needed to study the clinical evaluation and potential benefits of the improved resolution of the proposed approach in a larger cohort with well-defined coronary artery disease. We also note that the average navigator gating efficiency of most patient populations are around 30%–50%, which is lower than that of the healthy cohort in this study, and this will lead to longer

scan times. The reconstruction time of the proposed algorithm is too long for routine clinical use. As with other CS studies, we have not provided absolute SNR/contrast-to-noise-ratio measurements comparing the two reconstructions, as a reliable characterization of the noise signal is not available for the nonlinear CS reconstruction techniques (21,29).

CONCLUSION

We have demonstrated that a B_1-weighted LOST technique provides 6-fold acceleration of sub-mm whole heart coronary MRI, resulting in scan times of ~6 min. For such low SNR applications, the proposed CS approach with random undersampling may be more appropriate than parallel imaging with uniform undersampling.

APPENDIX: A

PROFILE ORDERING FOR RANDOM UNDERSAMPLING OF K-SPACE

We summarize the profile ordering for random k-space undersampling described in (21) for completeness. First, a pseudo-random k_y–k_z undersampling mask is generated, which includes the center of k-space of pre-defined size. In a segmented acquisition, the k-space lines from this mask are divided into different shots, where a shot is a group of lines that are acquired in one heartbeat. Each shot of the segmented coronary MRI acquisition, 20–25 k_y–k_z lines are sampled depending on the length of the subject-specific acquisition window. The division of the lines into different shots, and the acquisition order of the lines within each shot follows a specific profile ordering scheme: (1) Each k-space line is assigned magnitude and phase values based on its location in k_y–k_z plane (i.e., magnitude $= \mathrm{sqrt}(k_y^2 + k_z^2)$ and phase $= \mathrm{atan}(k_z/k_y)$), (2) Lines are assigned to different shots based on their phase values, such that a line with lower phase value is assigned to an earlier shot during the acquisition, 3) Within each shot, lines are sorted based on their magnitude values, such that a line with lower magnitude value is acquired first in the shot. As described in (21), this results in our proposed modified radial acquisition scheme that helps reducing the k-space jumps during the acquisition.

APPENDIX: B

IMPLEMENTATION DETAILS OF B_1-WEIGHTED LOST

The B_1-weighted LOST algorithm was implemented in two stages. For the first stage, the coil sensitivity information was used with total variation denoising to generate an initial image estimate. This was used for identification of similarity clusters, with parameters $N_b = 4$, $\lambda_{match} = 0.05$. For each reference block, comparison with other blocks was limited to a neighborhood of radius 6 in *x*–*y* and of radius 1 in *z* direction. The maximum number of blocks in a similarity cluster was limited to 8. During the second stage, data consistency using coil sensitivity information and LOST shrinkage were performed at every iteration, for a total of 25 iterations. For shrinkage, LOST alternated between hard thresholding and Wiener filtering, with thresholding parameters τ_{ht} and τ_{wie}, respectively, set to 0.015 and 0.02 times the largest coefficient of the estimate from the first stage.

REFERENCES

1. Lloyd-Jones D, Adams RJ, Brown TM, et al. Heart disease and stroke statistics—2010 update: a report from the American Heart Association. Circulation 2010;121:e46–e215.
2. Patel MR, Peterson ED, Dai D, Brennan JM, Redberg RF, Anderson HV, Brindis RG, Douglas PS. Low diagnostic yield of elective coronary angiography. N Engl J Med 2010;362:886–895.
3. Brittain JH, Hu BS, Wright GA, Meyer CH, Macovski A, Nishimura DG. Coronary angiography with magnetization-prepared T2 contrast. Magn Reson Med 1995;33:689–696.
4. Botnar RM, Stuber M, Danias PG, Kissinger KV, Manning WJ. Improved coronary artery definition with T2-weighted, free-breathing, three-dimensional coronary MRA. Circulation 1999;99:3139–3148.
5. Meyer CH, Hu BS, Nishimura DG, Macovski A. Fast spiral coronary artery imaging. Magn Reson Med 1992;28:202–213.
6. Bhat H, Ge L, Nielles-Vallespin S, Zuehlsdorff S, Li D. 3D radial sampling and 3D affine transform-based respiratory motion correction technique for free-breathing whole-heart coronary MRA with 100% imaging efficiency. Magn Reson Med 2011;65:1269–1277.
7. Hu P, Chuang ML, Ngo LH, Stoeck CT, Peters DC, Kissinger KV, Goddu B, Goepfert LA, Manning WJ, Nezafat R. Coronary MR imaging: effect of timing and dose of isosorbide dinitrate administration. Radiology 2010;254:401–409.
8. Nezafat R, Ouwerkerk R, Derbyshire AJ, Stuber M, McVeigh ER. Spectrally selective B1-insensitive T2 magnetization preparation sequence. Magn Reson Med 2009;61:1326–1335.
9. van Elderen SG, Versluis MJ, Westenberg JJ, Agarwal H, Smith NB, Stuber M, de Roos A, Webb AG. Right coronary MR angiography at 7 T: a direct quantitative and qualitative comparison with 3 T in young healthy volunteers. Radiology 2010;257:254–259.
10. Gharib AM, Abd-Elmoniem KZ, Herzka DA, Ho VB, Locklin J, Tzatha E, Stuber M, Pettigrew RI. Optimization of coronary whole-heart MRA free-breathing technique at 3 Tesla. Magn Reson Imaging 2011;29:1125–1130.
11. Knuesel PR, Nanz D, Wolfensberger U, Saranathan M, Lehning A, Luescher TF, Marincek B, von Schulthess GK, Schwitter J. Multislice breath-hold spiral magnetic resonance coronary angiography in patients with coronary artery disease: effect of intravascular contrast medium. J Magn Reson Imaging 2002;16:660–667.
12. Paetsch I, Jahnke C, Barkhausen J, Spuentrup E, Cavagna F, Schnackenburg B, Huber M, Stuber M, Fleck E, Nagel E. Detection of coronary stenoses with contrast enhanced, three-dimensional free breathing coronary MR angiography using the gadolinium-based intravascular contrast agent gadocoletic acid (B-22956). J Cardiovasc Magn Reson 2006;8:509–516.
13. Prompona M, Cyran C, Nikolaou K, Bauner K, Reiser M, Huber A. Contrast-enhanced whole-heart MR coronary angiography at 3.0 T using the intravascular contrast agent gadofosveset. Invest Radiol 2009;44:369–374.
14. Goldfarb JW, Edelman RR. Coronary arteries: breath-hold, gadolinium-enhanced, three-dimensional MR angiography. Radiology 1998;206:830–834.
15. Zheng J, Bae KT, Woodard PK, Haacke EM, Li D. Efficacy of slow infusion of gadolinium contrast agent in three-dimensional MR coronary artery imaging. J Magn Reson Imaging 1999;10:800–805.
16. Li D, Carr JC, Shea SM, Zheng J, Deshpande VS, Wielopolski PA, Finn JP. Coronary arteries: magnetization-prepared contrast-enhanced three-dimensional volume-targeted breath-hold MR angiography. Radiology 2001;219:270–277.
17. Weber OM, Martin AJ, Higgins CB. Whole-heart steady-state free precession coronary artery magnetic resonance angiography. Magn Reson Med 2003;50:1223–1228.

18. Bi X, Carr JC, Li D. Whole-heart coronary magnetic resonance angiography at 3 Tesla in 5 minutes with slow infusion of Gd-BOPTA, a high-relaxivity clinical contrast agent. Magn Reson Med 2007;58:1–7.
19. Hu P, Chan J, Ngo LH, et al. Contrast-enhanced whole-heart coronary MRI with bolus infusion of gadobenate dimeglumine at 1.5 T. Magn Reson Med 2011;65:392–398.
20. Yang Q, Li K, Liu X, Bi X, Liu Z, An J, Zhang A, Jerecic R, Li D. Contrast-enhanced whole-heart coronary magnetic resonance angiography at 3.0-T: a comparative study with X-ray angiography in a single center. J Am Coll Cardiol 2009;54:69–76.
21. Akcakaya M, Basha TA, Chan RH, Rayatzadeh H, Kissinger KV, Goddu B, Goepfert LA, Manning WJ, Nezafat R. Accelerated contrast-enhanced whole-heart coronary MRI using low-dimensional-structure self-learning and thresholding. Magn Reson Med 2012;67:1434–1443.
22. Gharib AM, Abd-Elmoniem KZ, Ho VB, Fodi E, Herzka DA, Ohayon J, Stuber M, Pettigrew RI. The feasibility of 350 μm spatial resolution coronary magnetic resonance angiography at 3 T in humans. Invest Radiol 2012;47:339–345.
23. Bhat H, Yang Q, Zuehlsdorff S, Li K, Li D. Contrast-enhanced whole-heart coronary magnetic resonance angiography at 3 T with radial EPI. Magn Reson Med 2011;66:82–91.
24. Tang L, Merkle N, Schar M, Korosoglou G, Solaiyappan M, Hombach V, Stuber M. Volume-targeted and whole-heart coronary magnetic resonance angiography using an intravascular contrast agent. J Magn Reson Imaging 2009;30:1191–1196.
25. Nagata M, Kato S, Kitagawa K, Ishida N, Nakajima H, Nakamori S, Ishida M, Miyahara M, Ito M, Sakuma H. Diagnostic accuracy of 1.5-T unenhanced whole-heart coronary MR angiography performed with 32-channel cardiac coils: initial single-center experience. Radiology 2011;259:384–392.
26. Niendorf T, Hardy CJ, Giaquinto RO, et al. Toward single breath-hold whole-heart coverage coronary MRA using highly accelerated parallel imaging with a 32-channel MR system. Magn Reson Med 2006;56:167–176.
27. Block KT, Uecker M, Frahm J. Undersampled radial MRI with multiple coils. Iterative image reconstruction using a total variation constraint. Magn Reson Med 2007;57:1086–1098.
28. Lustig M, Donoho DL, Pauly JM. Sparse MRI: the application of compressed sensing for rapid MR imaging. Magn Reson Med 2007;58:1182–1195.
29. Vasanawala SS, Alley MT, Hargreaves BA, Barth RA, Pauly JM, Lustig M. Improved pediatric MR imaging with compressed sensing. Radiology 2010;256:607–616.
30. Akcakaya M, Basha TA, Goddu B, Goepfert LA, Kissinger KV, Tarokh V, Manning WJ, Nezafat R. Low-dimensional-structure self-learning and thresholding: regularization beyond compressed sensing for MRI reconstruction. Magn Reson Med 2011;66:756–767.
31. Akcakaya M, Rayatzadeh H, Basha TA, Hong SN, Chan RH, Kissinger KV, Hauser TH, Josephson ME, Manning WJ, Nezafat R. Accelerated late gadolinium enhancement cardiac MR imaging with isotropic spatial resolution using compressed sensing: initial experience. Radiology 2012;264:691–699.
32. Wang Y, Riederer SJ, Ehman RL. Respiratory motion of the heart: kinematics and the implications for the spatial resolution in coronary imaging. Magn Reson Med 1995;33:713–719.
33. Danias PG, Stuber M, Botnar RM, Kissinger KV, Edelman RR, Manning WJ. Relationship between motion of coronary arteries and diaphragm during free breathing: lessons from real-time MR imaging. AJR 1999;172:1061–1065.
34. Otazo R, Kim D, Axel L, Sodickson DK. Combination of compressed sensing and parallel imaging for highly accelerated first-pass cardiac perfusion MRI. Magn Reson Med 2010;64:767–776.
35. Akcakaya M, Nam S, Hu P, Moghari MH, Ngo LH, Tarokh V, Manning WJ, Nezafat R. Compressed sensing with wavelet domain dependencies for coronary MRI: a retrospective study. IEEE Trans Med Imaging 2011;30:1090–1099.
36. Kim WY, Danias PG, Stuber M, et al. Coronary magnetic resonance angiography for the detection of coronary stenoses. N Engl J Med 2001;345:1863–1869.
37. Etienne A, Botnar RM, Van Muiswinkel AM, Boesiger P, Manning WJ, Stuber M. "Soap-Bubble" visualization and quantitative analysis of 3D coronary magnetic resonance angiograms. Magn Reson Med 2002;48:658–666.
38. Deriche R. Fast algorithms for low-level vision. IEEE Trans Pattern Anal Mach Intell 1990;12:78–87.
39. Otazo R, Xu J, Axel L, Sodickson D. Combination of compressed sensing and parallel imaging for highly-accelerated 3D first-pass cardiac perfusion MRI. In Proceedings of the 18th Scientific Meeting of ISMRM, Stockholm, Sweden, 2010. p. 344.
40. Kim YC, Narayanan SS, Nayak KS. Accelerated three-dimensional upper airway MRI using compressed sensing. Magn Reson Med 2009;61:1434–1440.
41. Feng L, Srichai MB, Lim RP, Harrison A, King W, Adluru G, Dibella EV, Sodickson DK, Otazo R, Kim D. Highly accelerated real-time cardiac cine MRI using k-t SPARSE-SENSE. Magn Reson Med 2012. doi: 10.1002/mrm. 24440.
42. Kim D, Dyvorne HA, Otazo R, Feng L, Sodickson DK, Lee VS. Accelerated phase-contrast cine MRI using k-t SPARSE-SENSE. Magn Reson Med 2012;67:1054–1064.
43. Kwak Y, Nam S, Akcakaya M, Basha TA, Goddu B, Manning WJ, Tarokh V, Nezafat R. Accelerated aortic flow assessment with compressed sensing with and without use of the sparsity of the complex difference image. Magn Reson Med 2012. doi: 10.1002/mrm. 24514.
44. Pruessmann KP, Weiger M, Bornert P, Boesiger P. Advances in sensitivity encoding with arbitrary k-space trajectories. Magn Reson Med 2001;46:638–651.